# HYDROCARBON FUEL PROCESS ANALYSIS
# BY ACOUSTO OPTIC TUNABLE FILTER
# NEAR INFRA-RED SPECTROSCOPY

Don Muller
Bran+Luebbe, Inc.
1025 Busch Parkway
Buffalo Grove, IL   60089
telephone   847-520-0700

## ABSTRACT

Octane and other properties of gasoline have been measured by near infra-red (NIR) spectroscopy since the laboratory trials at Technicon in the early 1980s. Over the past decade, systems have been developed for industrial process analysis. Acousto optic tunable filter (AOTF) is one of the NIR instrument technologies which has survived as appropriate for petrochemical process service. NIR spectroscopy is often the process analysis method of choice because of the speed of results and AOTF is one of the fastest NIR methods.

NIR spectroscopy is used for gasoline, diesel, and other hydrocarbon fuels as well as chemical and polymer process lines. One NIR sensor and instrument measures multiple properties -- octane, aromatics, vapor pressure, boiling points, and others of interest. The instrument is connected to sampling probes and cell at remote sites with fiber optics which can be used in the NIR. We have learned from experience which probes and sampling systems give good results. A double fiber optic and probe system provides the benefits of stable double beam spectroscopy.

Several chemometric systems have been used to develop the calibration equations required for NIR analysis. Those providing robust transferable calibrations will be presented.

## INTRODUCTION

Because the ASTM research octane number (RON) and motor octane number (MON) knock engines (1,2) are lengthy procedures not usually done at-line and have poor precision, they are not the best for refinery process control. NIR spectroscopy is more appropriate for process monitoring and control measurements.

Whether in a laboratory, near a process line, at-line, or on-line; NIR is a process analysis and control technology. Calibration development from samples of known composition is required. Once the calibration equation(s) are established, spectroscopic answers are provided in seconds

Electronic transitions in the visible and ultraviolet spectral region and molecular vibrational transitions in the infra-red (IR) region absorb so much energy that dilutions or very thin samples are required. This means that sample preparation and handling are required as part of any spectroscopic procedure, The NIR transitions are overtones and combination bands of the fundamentals IR vibrational transitions. They are thus much weaker and reasonably convenient pathlengths can be used with no sample preparation.

NIR spectroscopy measures absorbance at more than one wavelength. One or more can be used as a constant reference signal. This provides the stability and precision for NIR which is either lacking or has to be achieved in some other way for other on-line instrumental technologies.

## EXPERIMENTAL

### Instrumentation

There are several different technologies for producing NIR spectra for instrumental analysis. The heart of an AOTF spectrometer is the tellurium dioxide crystal shown in

Figure 1. The incident beam is from a quartz halogen source lamp. The lithium niobate transducer converts a radio frequency (RF) signal into untrasonic waves in the AOTF crystal. The frequency (wavelength) of the resultant tuned spectral beams depends on the wavelength of these ultrasonic waves (the acousto optic effect). Hence, as quickly and as accurately as the RF signal can be changed produces tuned beams of changed wavelength with no moving parts.

These tuned beams are sent through glass fiber optics to a sample probe up to hundreds of feet away and back to matched detectors in the instrument. One beam goes through the sample and the other is used as a reference beam. This provides the stable signal of double beam spectrophotometry. Flow through cells are provided on bypass lines or probes can be inserted into the main piping or vessel depending on the particular installation..

## Calibration & Chemometrics

For calibration development, full spectra are taken as shown in Figure 2. For our example of MON, the knock engine reference measurements for the same samples are required. Software is used to drive the instrument for spectra collection and data regression to product calibration equations. Principle component regression (PCR) or partial least squares (PLS) calibrations use all or part of the full spectrum of usually several hundred data points. Multiple linear regression (MLR) selects the best few (usually 2 to 6) wavelengths from the spectra.

For almost all of the applications mentioned below, MLR provided the calibrations most robust for analyzing samples once the calibration has been established. This is because the selected wavelengths are the ones due to the components being measured. Interferences and variations due to other factors in other parts of the spectra do not influence the predicted answer.

## Applications

The Bran+Luebbe InfraPrime was designed as an industrial environment system for liquid measurement in the refining and petrochemical industry, The most common installations are to measure those properties used to control motor fuel refineries: RON, MON, RVP, density, and characteristic distillation points. NIR nicely provides all these analyses from one spectrum. One calibration equation is used for each property measured. Several sites have added aromatics and PONA as measured properties.

Cetane number, boiling points, cloud point, freezing point, flash point, and CFPP are being measured for diesel fuel and kerosene production. Some of the calibration statistics are not as good for some of these properties because of the less precise nature of the reference analysis methods.

Sulfur, viscosity, and heat content are being measured at heavy fuel operations.

A wide range of applications are being used In polymer and chemical industries,. Less than 0.1 % additives are measured and controlled in high pressure and temperature extruders. Major components in polymerization reactors are being controlled. Physical properties such as viscosity are regularly being measured.

## RESULTS AND DISCUSSION

The prediction plot (Figure 3) shows how well the resulting NIR calibration and instrument agree with the reference knock engine for measuring MON. For this particular example, the standard error of the calibration samples was 0.18 MON and a standard error on predicting samples not in the calibration set of 0.22 MON. These are well within the variability of the MON knock engine method. NIR is often more precise than the reference method which generated the calibration set data.

The installation has been monitoring MON with on-line answers at this accuracy every 1.25 seconds continuously since August 1993. Several systems have been functioning for over 30,000 hours. With years of on-line design, installation, and evaluation experience; AOTF NIR spectroscopic systems have lived to their exciting promise as a technology for the on-line quality and process control of hydrocarbon fuels.

## REFERENCES

(1) ASTM *Annual Book of ASTM Standards* **1995,** *05.02,* D2699 *Standard test Method for Knock Characteristics of Motor Fuels by the Research Method*
(2) ASTM *Annual Book of ASTM Standards* **1995,** *05.02,* D2700 *Standard test Method for Knock Characteristics of Motor Fuels by the Motor Method*
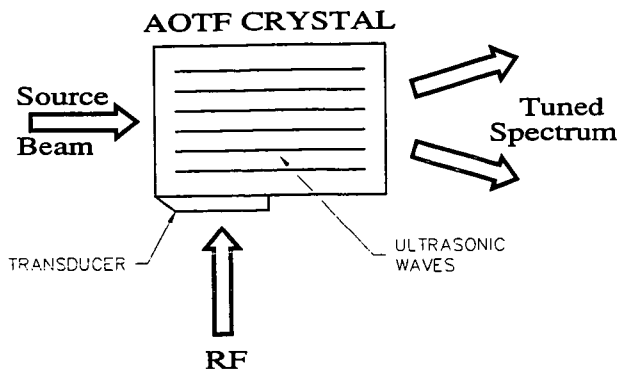(3) Tran, C.D.*Anal. Chem.* **1992,** *64,* 971A-981A

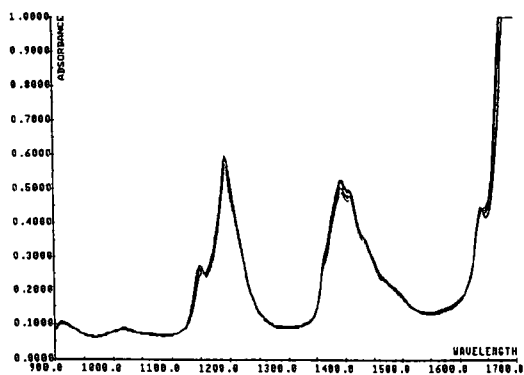**Figure 1.** AOTF: acousto optic tunable filter crystal spectroscopy



**Figure 2.** AOTF spectra of gasoline after the "naptha cracker" in a European refinery
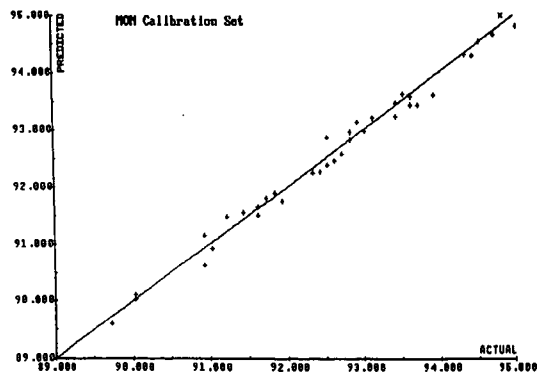


**Figure 3.** Prediction plot of MON precidcted by the NIR calibration model versus acual knock engine measured MON

# NEAR INFRARED SPECTROSCOPY FOR ON-LINE ANALYSIS OF ALKYLATION PROCESS ACIDS

Bruce B. Randolph, Senior Research Chemist, Process Support/Light Ends, CT Unit;
Alan D. Eastman, Senior Research Chemist, Molecular Structure Team, CT Unit;
Randall L. Heald, Special Problems Chemist, Refinery Laboratory, Borger Complex;

Phillips Petroleum Company, Bartlesville, OK 74004.

## INTRODUCTION

Alkylate, formed by the acid-catalyzed reaction of isobutane with C3-C5 olefins, is a key component for motor fuel blending. In the United States, current production is about $1 \times 10^6$ bbl/day, and represents 11-15% of the gasoline pool (somewhat higher in California).[1] Alkylate is comprised essentially of highly branched isoparaffins and has very high octane values, often in the 94-97 range for RON. It has low vapor pressure, narrow distillation range, and is essentially devoid of olefins, aromatics, and sulfur, making it the preferred blending component for reformulated gasolines (RFG). The demand for alkylate in the US is expected to lead to capacity expansions of 10-35%.[2]

HF alkylation is an important and widely-used process for making high-quality alkylate. Although the HF process has been used around the world for >50 years, efforts to optimize individual unit performance are always underway. Optimization can lead to significant economic advantage, since US capacity utilization is already 90%.[2]

The generally recognized advantages of on-line process monitoring, such as tighter process control, higher productivity, and improved product quality has led to much recent interest in this area. Continuous and immediate feedback of quantitative information is critical for optimized operation. These features are ideally suited for the alkylation process, where changes in the acid composition can occur more rapidly than can be observed with samples taken at normal intervals. Acid composition is important for optimal product quality, but until recently no on-line method existed for the determination of total acid composition.[3,4] Acid, water, and acid-soluble oil (ASO) concentrations are usually determined on intermittent samples taken to a laboratory. We have recently demonstrated the feasibility of using Near Infrared (NIR) spectroscopy for the on-line determination of HF, water, and ASO,[3] and here report application of those methods under continuous alkylation conditions.

## EXPERIMENTAL

The laboratory scale alkylation unit used in this work has been described previously.[3] The unit consists of a riser reactor, feed dispersion device, acid settler, acid recirculation pump, and product collection equipment.

The NIR data were collected with a flow cell mounted between the acid heat exchanger and acid pump; all of the acid inventory flows through the cell during each pass around the reactor. The cell was constructed of Hastelloy C alloy, using sapphire windows. For each run, a pre-blended feed of olefins and isobutane was introduced to the reactor.

Starting acid was 98% HF and 2% water by weight. The acid/hydrocarbon emulsion from the reactor is routed to the settler, where the acid phases out to the bottom and is recirculated to the reactor. Product hydrocarbon is withdrawn from the top of the settler, scrubbed to remove any HF, and collected for analysis. Acid samples were withdrawn intermittently for HF and ASO determination to provide a comparison for NIR values. All spectral data were collected using an Applied Automation Advance FT-IR. The instrument was coupled to the cell using 600 μm low-OH silica optical fiber. The data were processed using a partial least squares model developed from a calibration dataset described earlier.[3]

## RESULTS AND DISCUSSION

Selected results for Run #1 are given in Table 1. The feed was a blend of refinery-supplied olefins and isobutane, and a feed introduction device was chosen in order to increase the amount of ASO produced over that normally observed. This allowed enough ASO to be generated for a good comparison between NIR and standard techniques.

Standard HF titrations (dilution and titration to phenolpthalein endpoint) gave values within 2-3 wt% of the NIR values. The ASO concentrations determined by extraction (after neutralization) were usually only 50-70% of the NIR values. This was expected because the NIR measures total ASO, while the extraction measures mostly heavier ASO (*vide infra*). Water was not analyzed by an independent method; however the concentrations determined by NIR varied within a fairly narrow range (1.8 and 2.2 wt%). Figure 1 shows the trend lines associated with HF, ASO, and water at increasing times on stream.

After 92 hours, the feed was spiked with 570 ppm MTBE (or ~7000 ppm based on olefin only). MTBE is commonly produced upstream of the alkylation unit as an oxygenate for RFG. Under normal operation the concentration of MTBE in the alkylation feed is nil, but under upset conditions, levels of 1000-5000 ppm can have rapid, deleterious consequences for acid purity due to accelerated ASO production. Table 2 gives the results for the acid analysis at selected times on stream. Again the HF values from NIR are within 1-2 wt% of the titration values. Note the 70% increase in ASO concentration between 92 hours (table 1) and 113 hours (table 2), reflecting the high propensity for ASO production from MTBE. The increase in ASO based on traditional data was only ~33%. Both the NIR and traditional data show an increase in ASO with time, but again with traditional tests we observed only ~50-65% of the total ASO determined by NIR. Water remained relatively constant until purity was increased after 167 hours. At this time, the catalyst was nearly deactivated, necessitating a reduction of ASO and water and an increase in HF concentration. Figure 2 shows the trend lines for HF, ASO, and water with the MTBE-containing feeds.

One of the key advantages of NIR is the fast response time; in the present work spectra were taken every six minutes (times as short as 1 minute are possible). The inherent precision of NIR is another significant advantage, showing a 30- to 50- fold improvement in repeatability when compared to the traditional laboratory test methods for HF, water, and ASO. The current technique allows the rapid determination of HF, ASO, and water *directly* and *independently* of each other, in the presence of other dissolved/dispersed non-ASO hydrocarbons (C3, iC4, nC4, C5+ alkylate, etc.). This is a result of the method in which the training set data was collected. The NIR results add to 94% since the raw data was normalized to reflect the usual rule of 6% hydrocarbon dissolved/dispersed in the acid phase. In all cases, the sum of the raw data for HF, ASO, and water was between 99.6 and 100.1%, even though the model was *not* constrained to give that result. In traditional analyses, the difference between 94% and the sum of the acid components is taken as an indication of light ASO. As these data show, the traditional tests gave an indication of ~1-3% light ASO (the titration value of 93% at 44 hours is likely an outlier). The NIR technique is set up (by design) to measure both light and heavy ASO. This is the reason for the discrepancy between NIR and extraction measurements. Lighter ASO components are frequently lost during sample preparation for traditional tests.

The "spikes" present in Figures 1 and 2 occurred when acid was either added to or withdrawn from the reactor. These spikes in the trend lines result from the formation of gas/vapor bubbles which form inside the cell. Nitrogen is used as a pressure source for acid addition and to maintain constant unit pressure. As acid is withdrawn or added, a pressure differential results. The cell, which is located between the acid cooler and the magnetically driven acid recirculation gear pump, is susceptible to N2 gas bubble formation in the acid line. If bubbles develop, they can easily be trapped in the cell, since all of the acid in the system is routed through the cell. The gas bubbles cause rapid changes in the optical pathlength, resulting in wildly fluctuating values. The bubbles could be removed from the system by manipulation of the acid flow rate. Gas/vapor bubble formation is a phenomenon related to the experimental set-up in the laboratory, and proprietary equipment has been designed to eliminate their formation.

CONCLUSIONS
NIR appears to be ideally suited for on-line analysis of circulating acid in alkylation units. The fast response times, improved repeatability, and ability to provide quantitative information on HF, ASO, and water directly and independently in circulating acid represents a significant improvement over traditional methods of analysis.

REFERENCES

1. Rao, P., Vatcha, S.R., *Oil & Gas Journal*, 94(*37*), 56 (1996).

2. Rhodes, A., *Oil & Gas Journal*, 92(34), 49 (1994).

3. Heald, R.L., Randolph, B.B., Eastman, A.D., "NPRA National Meeting", March 16-18, 1997, San Antonio, TX, paper AM-97-57.

4. Ramamoorthy, P., US Patent 5,681,749, October 28, 1997.

Table 1. NIR and Traditional Acid Test Results: MTBE-Free Feed

| TOS (Hours) | 20 | 44 | 68 | 92 |
|---|---|---|---|---|
| %HF (titration) | 89.3 | 93.0 | 86.6 | 88.4 |
| %ASO (extn) | 0.85 | 1.25 | 2.09 | 2.52 |
| %H2O (NIR) | 1.80 | 2.0 | 2.19 | 2.16 |
| TOTAL | 92.0 | 96.3 | 90.9 | 93.0 |
| | | | | |
| %HF (NIR) | 91.81 | 90.22 | 88.69 | 88.02 |
| %ASO (NIR) | 0.391 | 1.78 | 3.12 | 3.92 |
| %H2O (NIR) | 1.80 | 2.00 | 2.19 | 2.06 |
| TOTAL | 94.0 | 94.0 | 94.0 | 94.0 |

Table 2. NIR and Traditional Acid Test Results: 570 ppm MTBE In Feed

| TOS (Hours) | 113 | 143 | 167 | 191 |
|---|---|---|---|---|
| %HF (titration) | 87.3 | 86.4 | 84.2 | 86.0 |
| %ASO (extn) | 3.35 | 4.0 | 4.7 | 4.7 |
| %H2O (NIR) | 2.01 | 2.08 | 2.01 | 1.78 |
| TOTAL | 92.7 | 92.5 | 90.9 | 92.5 |
| | | | | |
| %HF (NIR) | 85.3 | 84.4 | 83.3 | 85.0 |
| %ASO (NIR) | 6.71 | 7.51 | 8.73 | 7.28 |
| %H2O (NIR) | 2.01 | 2.08 | 2.01 | 1.78 |
| TOTAL | 94.0 | 94.0 | 94.0 | 94.0 |

# PLANAR LIQUID AND GAS VISUALIZATION[*]

Lynn A. Melton
Department of Chemistry
University of Texas at Dallas
Richardson, TX 75083-0688

## INTRODUCTION

Over the past decade, a variety of fluorescent diagnostic
systems, based on the photophysics of organic molecules and
intended for use in planar laser induced fluorescence (PLIF)
measurements of heating, evaporation, mixing, and flow
visualization in hydrocarbon liquids and vapors, have been
developed. These organic dopants interact with their
surroundings, either through concentration-dependent effects such
as quenching or through physical effects such as temperature and
polarity, and reveal information about the surroundings through
their fluorescence. The intent in this paper is to describe the
photophysical principles on which the systems are based, to
describe engineering applications (currently within the
combustion/mechanical engineering community), and to explore
applications of these and related diagnostics within the chemical
process industry. While there exist many applications of
fluorescence within the diagnostic community, this paper is
restricted to a review of the photophysics and applications of
these four novel systems, which have are not yet widely known in
the chemical process area.

The fluorescent diagnostic systems make use of PLIF
measurements of intensity and/or fluorescent lifetimes; they fall
into five broad categories:

(1) **exciplex-based vapor/liquid visualization** (EBVLV) systems,
which are now available for automotive as well as for diesel and
gas turbine fuels, make use of the photophysics of organic
exciplexes in order to provide spectrally-separated emissions
from the vapor and liquid phases.[1-4]

(2) **fluorescence shift thermometry** (FST) systems also make use
of the photophysics of organic molecules; these systems use
either the ratio of the emissions from the exciplex to that from
the excited monomer or the shift of the fluorescence band, both
of which are temperature-dependent, as an optical liquid phase
thermometer.[5-6] Such thermometers have been used to track the
temperature of falling, sub-millimeter diameter droplets in
experiments directed toward understanding heat transfer from a
hot gas to cold droplets.

(3) **streamlines by oxygen quenching** (SOQ), a technique which
exploits the efficient quenching of the fluorescence of organic
molecules by oxygen has been used in connection with **droplet
slicing imaging** (DSI) to provide dramatic qualitative evidence of
the existence of internal circulation patterns within falling,
sub-millimeter diameter droplets.[7]

(4) **fluorescence lifetime imaging** (FLI) requires the use of fast
dual gated image intensifiers to obtain two PLIF images, one a
few nanoseconds after the first. Quenching results in a
reduction of the fluorescence intensity **and** a reduction of the
fluorescence lifetime. The two images make it possible, in
principle, to obtain a lifetime image and, after appropriate
calculations, an intensity image, completely corrected for
quenching.[8] To date, the technique has been applied (a) to
fuel/oxygen equivalence ratio imaging (ERI),[9] and (b) to vapor
phase temperature imaging (VTI)[10].

(5) **film thickness imaging** (FTI)

Fluorescent thickness imaging is under development. In this
method the fluorescence of a molecule which has almost the same
volatility as automotive gasoline will be used to track the
evaporation of films of automotive gasolines. The system is used
in an optically thin configuration, and the fluorescence
intensity in a pixel is thus proportional to the film thickness.

## PHOTOPHYSICS OF FLUORESCENT DIAGNOSTICS

### A. processes

A recent review article discusses the photophysics of these combustion-related fluorescent diagnostics, and their fundamental limitations (volatility, quenching, etc.), in detail.[11]

### B.   excited state complexes

An exciplex or excimer [excited state complex or excited state dimer, denoted E* and called exciplex, unless the distinction is required] is formed in the reaction of an electronically excited molecule M* with an appropriate ground state molecule G (for excimers G = M), as shown in eqn. 1.[12]

$$M* + G(M) <==> E* \qquad\qquad (1)$$

E* may be bound by as much as 20-40 kJ/mole with respect to separated M* and G(M). Since there is no significant chemical binding of the ground state components of E*, and there may even be significant repulsion at the distance at which E* is most strongly bound, the fluorescence from E* is necessarily red-shifted with respect to the fluorescence of the excited monomer M*. The concentrations of M and G in the liquid can be adjusted to that the E* emission dominates in the liquid. The exciplex is unstable in the vapor phase, and thus the M* emission dominates in the vapor. Consequently, filters which isolate the E* and M* emission allow separate PLIF visualization of the liquid and vapor phases, respectively.

The reaction shown in equation (1) is temperature dependent, and the temperature dependence of the E*/M* intensity ratio can be exploited to make exciplex thermometers, which allow PLIF imaging of liquid phase temperatures within a few degrees over the temperature range 20 - 400 $^{\circ}$C.

### C.   apparatus for PLIF

Most PLIF experiments make use of a pulsed laser (in order to provide time resolution of the flow phenomena under study) whose beam is formed, via cylindrical lenses, into a sheet which is a fraction of a millimeter thick and 5-10 cm wide. Typically the fluorescence from the flow is imaged onto a CCD array camera which is placed at 90$^{\circ}$ to the plane of the exciting laser sheet. The choice of laser is determined by the wavelengths required for excitation of the fluorescent dopants. Most studies have used nitrogen lasers (337 nm) or Nd:YAG lasers (third harmonic at 355 nm or fourth harmonic at 266 nm). This apparatus is generic and the specificity of the diagnostic is gained through choice of the fluorescent dopant system(s).

## APPLICATIONS OF FLUORESCENT DIAGNOSTICS

### A.   exciplex-based vapor/liquid visualization

The best characterized, and most often applied, EBVLV system uses 0.5-1% (w/w) N,N,N',N'-tetramethyl-p-phenylenediamine (TMPD), nbp = 265 $^{\circ}$C/10% (w/w) naphthalene, nbp = 218 $^{\circ}$C/balance alkane (decane, tetradecane, or hexadecane). The liquid phase emission is dominated by the E* emission (peak at 480 nm), and the vapor phase emission is dominated by the M* emission (peak at 390 nm). Thus it is possible, by use of relatively broad-band filters to obtain separate images of the liquid or vapor phases in an evaporating fuel spray.

Most of the current applications of EBVLV have been in research automotive engines. Two examples are particularly noteworthy. Bardsley et al. acquired images for "diesel" and "automotive" sprays in a research engine, which was motored on nitrogen.[13-14] Shimizu et al. achieved near-quantitative use of an EBVLV system by using the E* emission to show that the liquid had completely evaporated. They were then able to calibrate the vapor phase emission as a function of the mixture fuel/oxygen ratio and crank angle in their automotive test engine. As a result, the spatial dependence of the equivalence ratio in the

precombustion portion of the engine cycle was displayed quantitatively.[15]

### B. fluorescence shift thermometry

Fluorescence thermometry has been used with bulk liquids and droplets falling into heated nitrogen. Stufflebeam showed that, in sealed, bulk liquids, spatial resolution of less than 1 mm and temperature errors of less than 1 $^{O}$C could be achieved over the range 20 - 100 $^{O}$C.[16] "Proof of concept" measurements of the temperature of decane or hexadecane droplets falling into heated nitrogen have been carried out with illumination of (1) the entire cross section of an optically thick droplet ("whole droplet, skin temperature"),[17] (2) the entire cross section of an optically thin droplet ("whole droplet, volume averaged temperature"),[18] and (3) a central slice of the droplet ("droplet slicing, temperature field").[19] In more recent work, the evaporation of a fuel which had been sprayed onto a hot steel plate was followed through images of the temperature of the remaining liquid at intervals of a 0-100 msec after the injector was pulsed.[20]

### C. streamlines by oxygen quenching

The techniques of streamlines by oxygen quenching and droplet slicing imaging were developed for the purpose of testing whether aerodynamic drag on droplets of sizes typical of fuel sprays could induce internal circulation within the droplet, which circulation can dramatically alter the time required for the droplet to heat sufficiently for evaporation rates to become significant.[7] For SOQ, the droplet is formed from a solution which contains a dopant whose fluorescence is easily quenched by oxygen (typically naphthalene in decane) and which solution has been purged of oxygen. The droplet falls into an oxygen containing atmosphere, and oxygen contacts and diffuses into the surface liquid. For DSI, the laser beam is formed into a sheet which is narrow compared to the droplet diameter and which illuminates an equatorial plane of the droplet. SOQ/DSI measurements on droplets which have internal circulation show dark (oxygen containing, fluorescence quenched) streaks curving into the light droplet disk.[7]

### D. fluorescence lifetime imaging

In FLI, a rapid lifetime determination algorithm, which relies on two gated intensity images and the assumption that the fluorescence decay is a single exponential, allows the subsequent calculation of the fluorescence lifetime image.[21] The fluorescence image was split, and each portion passed through a fast gated imaged intensifier (off/on/off time selectable from 1 to 12 nsec, intensifiers and high voltage pulser system supplied by Grant Applied Physics, Berkeley, CA) and an appropriate filter. The two gated fluorescence signals were finally focused onto two halves of a single CCD camera (Photometrics Star-1).

The equivalence ratio (phi) is the ratio of the fuel vapor concentration to the oxygen concentration, normalized so that the equivalence ratio is unity when there is just sufficient oxygen present to burn all the fuel to water and carbon dioxide. phi < 1 is "fuel lean", and phi > 1 is "fuel rich".

For equivalence ratio imaging (ERI), further processing is required. As shown in equations (2a) and (2b), the Stern-Volmer equations for intensity and for lifetimes have the same right hand side.

$$I_0/I = 1 + K'[O_2] \tag{2a}$$

$$tau_0/tau = 1 + K'[O_2] \tag{2b}$$

where the "o" subscript denotes the quantity measured in the absence of the quencher, which here is $O_2$. In a non-homogeneous mixture of fuel with air, variations in intensity may arise either from variations in the distribution of the fuel (and with it the fluorescent dopant which was mixed into the fuel), or from variations in the amount of oxygen (and consequent variations in the amount of quenching), or both. One needs to determine the unquenched intensity image ($I_0$) in order to determine the

distribution of fuel, however, only the intensity image with quenching (I) is experimentally accessible. With prior knowledge of the fluorescence lifetime in the absence of quenching, and measurement, pixel-by-pixel, of the mixture lifetime, the right hand side of equations (2a) and (2b) can be determined, and thus the unquenched intensity image, in which the intensity is directly proportional to the fluorescent dopant concentration, can be obtained. With further knowledge that quenching by oxygen is the only significant means of shortening the fluorescence lifetime in the system under study and with measurement of the rate of quenching of the fluorescence by oxygen, the oxygen concentration image can be obtained. If the system has been prepared in such a fashion that the concentration of the fluorescent dopant is in a fixed and known ratio to the fuel vapor concentration, then pixel-by-pixel ratioing and subsequent scaling of the ratio yields an image of the fuel/oxygen equivalence ratio. This technique has been demonstrated in fluoranthene doped jets of methane into air; typical results are shown in Figure 7.[9]

For vapor temperature imaging, a fluorescent dopant whose lifetime is temperature sensitive is used. In this case a calibration curve of the fluorescence lifetime versus temperature is used to convert the fluorescence lifetime image to a vapor temperature image. The temperatures are obtained solely from lifetime data and do not depend upon the concentration of the fluorescent dopant so long as sufficient signal is obtained for accurate measurements. Since oxygen, particularly, also shortens the fluorescence lifetimes, it must be rigorously excluded in the VTI experiments. This technique has been demonstrated for a heated jet of naphthalene doped nitrogen at the center of a cold coflow of naphthalene doped nitrogen.[10]

**POTENTIAL APPLICATIONS IN THE CHEMICAL PROCESS INDUSTRY**

A significant drawback to the utilization of such fluorescent diagnostics in the chemical process industry is the sensitivity of the fluorescent dopants to quenching by molecules in the environment. It may be possible to show that the process stream does not contain significant quenchers, but this must be established on a case-by-case basis.

As described in the discussions of exciplex-based vapor/liquid visualization, exciplex fluorescence thermometry, streamlines by oxygen quenching, and fluorescence lifetime imaging, fluorescence measurements can also be generated under planar illumination conditions, and thus two-dimensional maps of a property field can be obtained. Thus fluorescence imaging is particularly useful for situations, such as studies of two phase flow or mixing, where such 2-D information is critical.

**REFERENCES**

1.   Melton, L.A., "Fluorescent Additives for Determination of Condensed and Vapor Phases in Multiphase Systems", U.S. Patent 4,515,896, issued May 7, 1985, assigned to United Technologies Corporation.

2.   Melton, L.A., "Spectrally Separated Fluorescence Emissions for Diesel Fuel Droplets and Vapor," *Appl. Opt.* **1983**, *22*, 2224.

3.   L.A. and Verdieck, J.F., "Vapor/Liquid Visualization for Fuel Sprays", *Combust. Sci. and Tech.* **1985**, *42*, 217.

4.   Melton, L.A., "Exciplex-Based Vapor/Liquid Visualization Systems Appropriate for Automotive Gasolines", *Appl. Spectrosc.* **1993**, *47*, 782.

5.    Melton, L.A., "Method for Determining the Temperature of a Fluid," U. S. Patent 4,613,237; issued September 23, 1986; assigned to United Technologies Corporation.

6.    Murray, A.M. and Melton, L.a., "Fluorescence Methods for Determination of Temperature in Fuel Sprays," *Appl. Opt.* **1984**, *24*, 2783.

7.    Winter. M. and Melton, L.A., "Measurement of Internal Circulation in Droplets Using Laser-Induced Fluorescence", *Appl. Opt.* **1990**, *29*, 4574.

8.    Ni, T.Q. and Melton, L.A., "Fluorescence Lifetime Imaging: An Approach for Fuel Equivalence Ratio Imaging", *Appl. Spectrosc.* **1991** *45*, 938

9.    Ni, T.Q. and Melton, L.A., "Fuel Equivalence Ratio Imaging for Methane Jets", *Appl. Spectrosc.* **1993**, *47*, 773.

10.   Ni, T.Q., and Melton, L.A., "2-D Gas Phase Temperature Measurement Using Fluorescence Lifetime Imaging", *Appl. Spectrosc.* **1996**, *50*, 1112.

11.   Melton, L.A., "Planar Laser and Gas Visualization", *Ber. Bunsenges. Phys. Chem.* **1993**, *97*, 1560.

12.   Birks, J.B., "Excimer Fluorescence in Organic Compounds," in Progress in Reaction Kinetics, G. Porter, Ed., **5**, (Pergamon, London, 1969).

13.   Bardsley, M.E.A., Felton, P.G., and Bracco, F.V., "2-D Visualization of Liquid Fuel Injection in an IC Engine", SAE Int. Congress and Exp., Feb. 29 - Mar. 4, 1988, paper 880521, (1988).

14.   Bardsley, M.E.A., Felton, P.G., and Bracco, F.V., "2-D Visualization of a Hollow-Cone Spray in a Cup-in-Head, Ported I.C. Engine", SAE Int. Congress and Exp., Feb. 27 - Mar. 3, 1989, paper 890315, (1989).

15.   Shimizu, R., Matumoto, S., Furuno, S., Murayama, M. and Kojima, S., "Measurement of Air-Fuel Mixture Distribution in a Gasoline Engine Using LIEF Technique", SAE Fuels and Lubricants Meeting, October 21-23, 1992, paper 922356, (1992).

16.   Stufflebeam, J.H., "Exciplex Fluorescence Thermometry of Liquid Fuel", *Appl. Spectrosc.* **1989**, *43*, 274.

17.   Wells, M.R., and Melton, L.A., "Temperature Measurement of Falling Droplets", *Trans. ASME: Journal of Heat Transfer* **1990**, *112*, 1008.

18.   Hanlon, T.R.,  and Melton, L.A., "Exciplex Fluorescence Thermometry of Falling Hexadecane Droplets", *Trans. ASME: Journal of Heat Transfer* **1992**, *114*, 450.

19.   Winter, M., "Measurement of the Temperature Field Inside a Falling Droplet", ILASS-Americas, 4th annual conference, Extended Abstracts, Hartford, CT (1990).

20.   Ni, T.Q., and Melton, L.a., in preparation.

21.   Ballew, R.M., and Demas, J.N., "An Error Analysis of the Rapid Lifetime Determination Method for the Evaluation of Single Exponential Decays", *Anal. Chem.* **1989**, *61*, 30.

# SENSOR SELECTION AND PLACEMENT FOR PROCESS CONTROL

**Charles F. Moore,** Arlene A. Garrison, Paul D. Hall
Measurement and Control Engineering Center
102 Estabrook Hall
University of Tennessee
Knoxville, TN 37996-2350

## ABSTRACT
Effective application of sensor technology in industrial processes requires careful attention to the optimal placement of the sensor. Available locations must be analyzed based upon potential leverage in a control scheme. After location is determined, the measurement need is clearly defined and the most appropriate sensor can be selected. Tools have been developed to assist in appropriate sensor placement. The use of the tools in distillation column applications will be discussed.

## INTRODUCTION
Raman spectroscopy provides a useful alternative for in-process vibrational spectroscopic analysis. Instrument vendors originally designed spectrometers for laboratory use, and recently systems have become available with NEMA enclosures and remote optical fiber capability. There are many potential process applications for these stable, easy to use instruments. Raman spectroscopy is highly suited to analysis of aqueous samples.

The Department of Energy has funded research at the Measurement and Control Center to establish the utility of Raman spectroscopy for on-line composition analysis in distillation columns. The Fourier Transform instrument selected employs an air-cooled laser and a thermoelectrically cooled detector. The device is mounted on a three by three foot cart for convenient location in control rooms. Current fiber optic extension cables allow for analysis in a cell thirty five meters from the instrument.

Application of the device to an acid recovery column at Eastman Chemical Company in Kingsport, Tennessee will be discussed. Sensor placement is critical to optimal application of any on-line device. Potential energy savings and product throughput increase will be outlined.

## EXPERIMENTAL
During the project a multiple point measurement system was constructed and tested.[1-5] This was accomplished by routing the excitation light from a diode pumped YAG laser to the measurement points with optical fibers and returning the Raman scattered light to the spectrometer with optical fibers. An optical multiplexer was designed to time-share the light in both paths. The excitation light wavelength was in the near infrared range, thereby reducing the possible fluorescence of the samples to be analyzed.

The spectrum of the Raman-scattered light was measured by use of an interferometer-based spectrometer, a Perkin-Elmer 1700 adapted for Raman use. The system was controlled by an INTEL based computer. The computer initiated a scan of the spectrum of the chemical stream, gathered the spectral data from the spectrometer and estimated the composition of the constituents. The calibration of the system was accomplished by a process in which multiple samples with different typical concentrations of the constituents of the chemical stream were analyzed and their spectra stored. Next, the unique set of orthogonal functions making up the experimental data were found. Finally an empirical mathematical model of the relation between spectral features and composition was formed based on multiple linear regression of the weights of the orthogonal functions against the known concentrations of the constituents. The accuracy goal of the project was a measurement of composition of each constituent of a process chemical stream within 3 minutes with a root-mean-square (rms) uncertainty of less than 2%. The final system achieved an error of about 1% rms in 3 minutes for the constituents composing the chemical stream in the field trial test site, Eastman Chemical Company of Kingsport, Tennessee.

Various composition analysis methods have been considered for use in column process control. Many methods have been utilized with varying degrees of success due to inherent limitations in these techniques. A critical concern in determining potential energy savings utilizing comp-

osition control is the universality of the on-line analyzer. Raman spectroscopy was chosen for this development effort as highly appropriate for the control of a broad range of distillation separations. Of the three common optical spectroscopic methods in use today, fluorescence spectroscopy, absorption spectroscopy, and Raman spectroscopy, Raman was selected because of its narrow, distinct spectral features and relative insensitivity to the presence of water in the sample.

One important aspect of composition based control systems is the relationship between the composition measurement location and the required measurement resolution. One feature of the Raman based composition analyzer is that it can be used to measure compositions internal to the distillation column. (Conventional process analyzers are typically applied to product streams). This offers several advantages for addressing the control and energy reduction problems. The first advantage is demonstrated in Figure 1, where the sensitivity of the composition profiles to changes in the reflux and steam is plotted against the height in the column. Note that product ends (where conventional analyzers are applied) have very little sensitivity. The leverage in controlling composition is orders of magnitude greater if the measurement is made inside the column. This is a characteristic of the Eastman column, but it is also a general characteristic of most distillation processes. If composition information is to be used in stabilizing a column, it needs to be well selected internal composition and not product compositions.

## RESULTS AND DISCUSSION
The projected economic analysis quantified the improvements in the Eastman column control that would be possible if the control system were based on composition measurements instead of temperature as was the prior practice. This preliminary study was conducted on a simulation of the proposed field test column and included two relatively simple composition control strategies. The results of the study indicate that there is a clear advantage to composition based control.[6] Both composition control schemes significantly reduced the variation in the product composition. Reducing variation saves energy by allowing operation of the column much closer to the minimum energy requirement without jeopardizing the product specification.

The cost of the analyzer vs. the anticipated energy savings was not specifically addressed in the economic analysis. The general feeling is that the cost of the components in the prototype system does not accurately reflect the price for an industrially hardened, commercial unit.

This study demonstrates that the high resolution and mechanical sampling requirements placed on present industrial analyzers are not necessary. High resolution and sampling both contribute to the capital as well as the maintenance costs of current process analyzers. A commercial Raman based analyzer should compete quite favorably with these existing technologies in both price and maintenance. Also, it should yield much higher control performance. The control performance advantage offered by the Raman based analyzer is that it can be applied with relatively little difficulty to determine the internal composition of the column.

## ACKNOWLEDGMENTS

## REFERENCES
1. M.J. Roberts, A.A. Garrison, S.W. Kercel, D.S. Trimble, C.F. Moore and E.C. Muly, "Development and Application of a Raman Spectroscopy Based Instrument for Multi-Point Composition Analysis and Control of a Distillation Column", ISA 90, New Orleans, LA, pp. 463-468, October 1990.

2. A.A. Garrison, D.S. Trimble, E.C. Muly, M.J. Roberts and S.W. Kercel, "On-Line Chemical Analysis Applied to Distillation Control - A Status Report", American Laboratory, pp. 19-27, February 1990.

3. A.A. Garrison, C.F. Moore, M.J. Roberts and P.D. Hall, Distillation Process Control using FT-Raman Spectroscopy, Process Control and Quality, 3 (1992) 57-63.

4. M.Z. Martin, A.A. Garrison, M.J. Roberts, P.D. Hall, and C.F. Moore, Composition Monitoring by On-Line Remote Raman Spectroscopy, Process Control and Quality, 5 (1993) 187-192.

5. A.A. Garrison and M.Z. Martin, Fourier Transform Raman Spectroscopy for Process Analysis, Proceedings of the Fourteenth International Conference on Raman Spectroscopy, Hong Kong, August, 1994, N.-T. Yu and X.-Y. Li, editors, 804-805.

6. Paul D. Hall, *Distillation SISO Control System Design and Analysis Using Internal Composition Measurements*, University of Tennessee Dissertation, 1994.
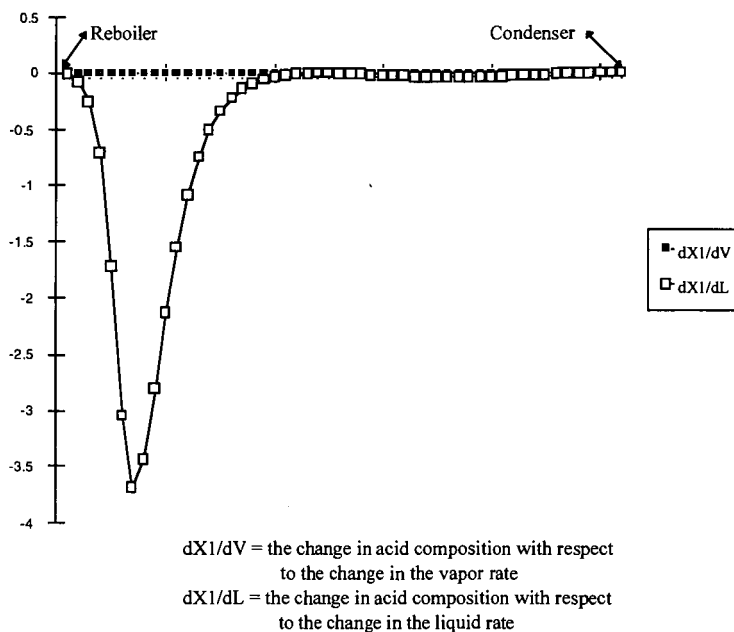
dX1/dV = the change in acid composition with respect
to the change in the vapor rate
dX1/dL = the change in acid composition with respect
to the change in the liquid rate

Figure 1
Acid Composition Sensitivity vs. Column height

# FIBER-OPTIC ARRAY SENSORS

Paul Pantano,* Anna A. Panova[†] and David R. Walt[†]
*Department of Chemistry, University of Texas at Dallas, Richardson, TX 75083
[†]and Department of Chemistry, Tufts University, Medford, MA 02155

## ABSTRACT

Despite many innovations and developments in the field of fiber-optic chemical sensors, optical fibers have not been employed to both view a sample and concurrently detect an analyte of interest. While chemical sensors employing a single optical fiber or a non-coherent fiber-optic bundle have been applied to a wide variety of analytical determinations, they cannot be used for imaging. Similarly, coherent imaging fibers have been employed only for their originally intended purpose, image transmission. Recently, we have used coherent imaging fibers to make fiber-optic chemical sensors. First, imaging fibers can be used to fabricate array sensors that can concurrently view a sample and detect a single analyte. Second, sensors can be made with spatially-discrete sensing sites for multianalyte determinations. Applications will include studying corrosion processes from remote locations.

## INTRODUCTION

An imaging fiber is comprised of thousands of individual 2-μm-diameter optical fibers that are melted and drawn together in a coherent manner such that an image can be transmitted from one end of the fiber to the other. These imaging fibers (200-500 μm in diameter) have been utilized to construct several types of novel chemical sensors.[1]

In one approach, we have demonstrated the ability to combine two types of useful measurements (visual and chemical) using a single imaging fiber.[2] A pH-sensitive fluorescent dye was incorporated into a porous polymer layer after it was spin-coated directly onto the distal surface of an imaging fiber. When the pH-sensitive layer was sufficiently thin (≤2 μm), the fiber's imaging capabilities were not compromised. By combining the distinct optical pathways of the imaging fiber with a charge coupled device, visual (white light) and chemical (fluorescence) measurements could be acquired concurrently with 4-μm-spatial resolution. This technique has many potential applications for remote in situ analyses. For example, recent work has involved imaging a copper/aluminum corrosion cell with a pH-sensitive imaging fiber.[3]

In another approach, discrete arrays of micrometer-sized sensing regions have been photodeposited onto the distal tip of a single imaging fiber.[4] Using a charge coupled device, the fluorescence from each of the different sensing regions immobilized on the imaging fiber could be spatially resolved. The creation of spatially discrete sensing sites on a single optical sensor solves many of the problems associated with designing multianalyte optical sensors such as spectral overlap of multiple indicators and the need to use individual optical fibers for each analyte. Simultaneous measurements are especially important in a number of environmental applications, especially when the dynamics of different analytes are closely interrelated (e.g., pH, $pCO_2$, and $pO_2$). This technique has many potential applications since numerous indicating chemistries (including those for metal ions) can be co-immobilized on a single imaging fiber to form compact multianalyte sensor arrays.

## EXPERIMENTAL

Approach #1: pH-sensor fabrication begins by successive polishing of the distal and proximal faces of a 350-μm-diameter imaging fiber (Sumitomo Electric Industries, Torrance, CA) with 30-μm, 15-μm, 3-μm and 0.3-μm lapping films (General Fiber Optics, Fairfield, NJ). Residual polishing material was removed by wiping the faces of the imaging fiber with an acetone-soaked cotton swab. The polished distal face of the imaging fiber required treatment to activate the glass surface with a polymerizable double bond. Surface activation was achieved by silanizing the fiber surface for 2 h using a 10% solution of 3-trimethoxysilylpropyl methacrylate in acetone. After rinsing the fiber with acetone, the surface-bound acrylate was cured at room temperature for a minimum of 30 min. This procedure functionalizes the surface with a polymerizable acrylate to facilitate adhesion of a photopolymer to the glass surface of the optical fiber. A thin layer of polyHEMA/N-fluoresceinylacrylamide was then polymerized at the distal tip using photochemical polymerization in conjunction with

spin coating methods. The stock photochemical polymerization solution consisted of 10 mL HEMA, 200 μL ethyleneglycol dimethacrylate, and 1 mL of dye solution (50 mg N-fluoresceinyl-acrylamide (synthesized from fluoresceinamine isomer I and acryloyl chloride) in 10 mL *n*-propanol). Individual solutions were prepared with 0.5-mL stock polymerization solution and 30 mg benzoin ethyl ether. Deoxygenated stock polymerization solution (100 mL) was stirred in a 6 x 50 mm test tube and prepolymerized with 366-nm light for 45 s. The resulting viscous oligomer was spread uniformly across the imaging fiber surface by placing a drop of it (approximately 1 mL) on the distal tip of a functionalized imaging fiber (held vertically in a Servodyne mixer head (Cole Parmer, Chicago, IL)) and spinning the fiber at 2000 RPM for 20 s. After spin coating, the polyHEMA/ fluorescein-modified imaging fiber was illuminated with 366-nm light for 1.5 min to complete the polymerization and bond formation. The modified epifluorescence microscope used for fluorescence measurements and imaging has been described previously.[2] The system is capable of making continuous ratiometric measurements through the use of a CCD camera and computer-controlled filter wheels and shutters. During fluorescence measurements, the filter wheels are positioned at the dye's excitation and emission maxima with the fluorescence images being captured by the CCD camera.

## RESULTS AND DISCUSSION

The main objective of this work is to create a planar array of thousands of optical sensors in a unitary, flexible fiber format. This approach benefits from the commercial availability of coherent imaging fibers comprised of thousands of micron-sized optical fibers fused together in a fixed arrangement. By coating one end of the imaging fiber with an analyte-sensitive material, we obtain thousands of microsensors capable of simultaneously measuring chemical concentrations with 4-μm spatial resolution over tens of thousands of square microns. In addition, the image carrying capabilities of the fiber are preserved allowing the operator both to position the sensor and to couple the chemical measurements to visual information.

Recent work has involved imaging a copper/aluminum corrosion cell with a pH-sensitive imaging fiber (Figure 1). In these experiments, the electrodes were placed in aqueous buffer and the distal end of the pH-sensitive imaging fiber was brought into contact with the metal surface. Fluorescence images were taken before and after the surface was exposed to a buffer solution with the change in fluorescence being attributed to the generation of hydroxide ion from the reduction of water that accompanies the anodic dissolution of a metal (Figure 2). Such studies provide information regarding the chemical and physical changes during the initial stages of corrosion.

## ACKNOWLEDGMENTS

## REFERENCES

[1] Pantano, P. and Walt, D. R. *Anal. Chem.* 1995, *67*, 481A-487A.
[2] Bronk, K. S.; Michael, K. L.; Pantano, P. and Walt, D. R. *Anal. Chem.* 1995, *67*, 2750-2757.
[3] Panova, A. A., Pantano, P. and Walt, D. R. *Anal. Chem.* 1997, *69*, 1635-1641.
[4] Healey, B. G.; Foran, S. E. and Walt, D. R. *Science* 1995, *269*, 1078-1080.
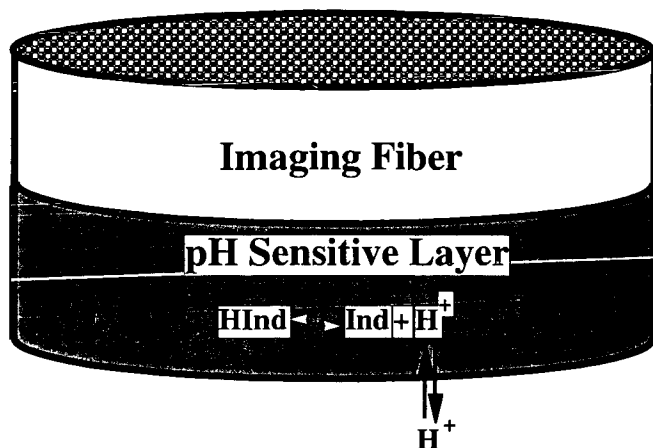
**Figure 1.** Schematic diagram of a pH-sensitive indicator immobilized to an imaging fiber's distal face.
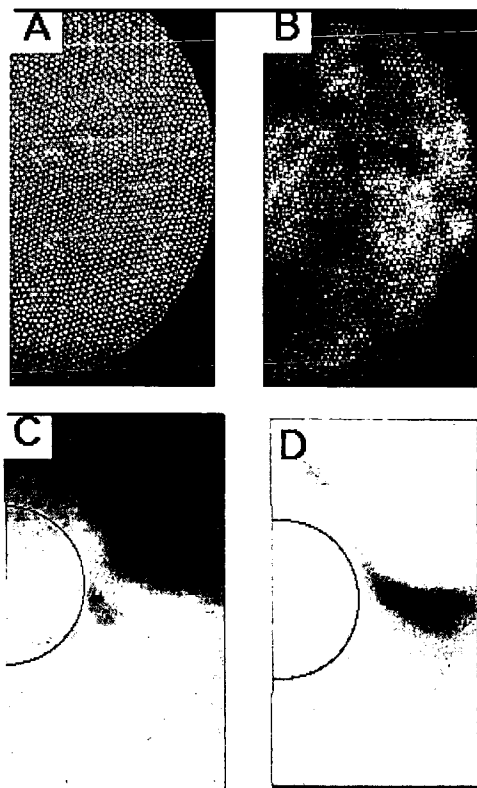


**Figure 2.** **(A)** fluorescence image taken at 490-nm excitation and 530-nm emission acquired through a pH-sensitive imaging fiber placed in contact with buffer. **(B-D)** images acquired through a pH-sensitive imaging fiber placed in contact a polished aluminum-clad copper wire (the image corresponds to half of the wire surface). **(B)** white light image, **(C)** fluorescence image after 1-min exposure of the metal surface to buffer, **(D)** background-subtracted fluorescence image taken after 5-min exposure. High fluorescence intensities (high pH) are denoted by white. The black half-circle denotes the Al/Cu border.

# CAN SOOT PRIMARY PARTICLE SIZE BE DETERMINED USING LASER-INDUCED INCANDESCENCE?

Thomas M. Ticich, A. Brock Stephens, Department of Chemistry,
Centenary College of Louisiana, Shreveport, Louisiana, 71134

Randy L. VanderWal, Nyma@NASA-Lewis Research Center,
Cleveland, Ohio 44315

laser-induced incandescence, soot, primary particle size

## ABSTRACT

We have obtained temporally-resolved laser-induced incandescence (LII) signals from different size primary particles produced by diffusion flames of methane, ethane, ethylene, and acetylene. These results represent the first direct comparison between primary particle sizes based on optical measurements and those directly measured through TEM. Two measures of the temporal decay of the LII signal reveal a correlation with primary particle size. Comparison between primary particle sizes based on the calibrations using the temporal analysis of the LII signal and TEM measurements reveal agreement within the growth region and very late in the oxidation region within an ethylene gas-jet diffusion flame. Significant differences exist at intermediate positions which likely represent the effects of cluster-cluster aggregation within the oxidation region.

## INTRODUCTION

Soot surface growth rather than nucleation has been found to dominate soot mass yield (1-4). Essential in characterizing the rate of soot growth and assessing theoretical models is the soot surface area. For example, soot mass proceeds via hydrogen abstraction creating a surface radical site in preparation for acetylene addition to the site (5). In such a process, the mass addition rate will depend upon total surface area in addition to the number of potential reactive sites (6).

Several parameters characterizing soot mass growth can be readily measured optically, such as soot volume fraction ($f_v$), velocity and temperature. Optical measurements are advantageous because they are non-intrusive and take place in real time. Optical, in-situ determination of primary particle size would further facilitate measuring soot mass growth and oxidation rates per unit surface area. The current methodology for primary particle size determination is through analysis of transmission electron microscopy (TEM) micrographs of thermophoretically sampled soot, an intrusive and time-intensive process (1-4).

Largely due to its high temporal and spatial resolution, laser-induced incandescence (LII) has advanced $f_v$ measurements to a wide range of combustion processes. Theoretical models of LII predict that the temporal evolution of the signal after the excitation laser pulse is dependent upon primary particle size (7-11). This is physically sensible given that the temporal evolution of the LII signal is dependent upon the cooling of the primary particles predominantly through conduction and convection, processes dependent upon surface area. Thus the work presented here seeks to explore the potential of LII for determining particle size. Given the number of assumptions utilized in present LII theoretical models regarding the physical and structural properties of the laser-heated soot (7-11), we adopted an empirical approach to seek a correlation between the temporal decay rate of the LII signal and primary particle size as determined from analysis of transmission electron micrographs of thermophoretically sampled soot.

## EXPERIMENTAL

A variety of laminar gas-jet diffusion flames produced by different fuels and flowrates were used to produce a wide range of primary particle sizes at similar temperatures and near the maximum in their growth history. Table 1 lists the different fuels, flow conditions, sampling heights above the burner, primary particle sizes and local temperatures for each of the four flames studied. The flame temperatures reported were measured by thermocouples employing rapid

insertion (*12*) with subsequent radiation correction (*13*). Each gas-jet diffusion flame was supported on a 10.5 mm I.D. nozzle surrounded by an air coflow through a 101 mm diameter honeycomb. A chimney with windows for optical access served to stabilize the flame and provide shielding from room drafts.

For LII measurements, the 1064 nm light from a pulsed Nd:YAG laser was formed into a 500 μm-wide sheet and directed through the flame. LII signals were relayed through a quartz optical fiber to a monochromator fitted with a photomultiplier tube (PMT) as the detector. The signal collection system has a spectral bandwidth of 12 nm and a transverse spatial resolution of 1 mm. Time-resolved PMT signals were sampled using a 500 MHz digital oscilloscope which also coaveraged 200 individual temporal scans.

Thermophoretic sampling provided soot samples for transmission electron microscopy. Probe residence times within the flames ranged from 30-60 ms depending on the soot volume fraction. TEM grids with ultrathin substrates aided visualization of the sampled soot. TEM micrographs were analyzed for primary particle size using commercial image processing software.

## RESULTS AND DISCUSSION

### Calibration Development

Figure 1 shows the time-resolved LII signal for three flames at the longest detection wavelength studied, 600 nm. Qualitatively similar data were obtained at shorter detection wavelengths but the largest observed variation in the temporal evolution of the LII signal occurred at 600 nm. Two analysis methods based on a theoretical model of the LII signal have been reported recently for extracting primary particle size from LII data (*10,11*). The first method uses the ratio of signal intensity (integrated over a specified time duration after the excitation laser pulse) at two detection wavelengths (*10*). An advantage of this method, according to the theoretical model, is reduced sensitivity to differences in ambient flame temperature. Analysis of our data in this manner, however, gave a nonmonotonic relationship between the ratio and primary particle size, which would result in a given signal ratio indicating two different particle sizes.

The second method of analysis is based on the ratio of signal intensity at a single detection wavelength with the signal integrated over selected electronic gate durations (*11*). Figure 2 shows the results of this method of analysis applied to the time-resolved LII signals from the different primary particle sizes. Because the method uses a limited portion of the experimental data, we also sought to utilize all the experimental data by fitting the signal decay to a mathematical function. Our analysis showed significant disagreement between the decaying portion of the time-resolved data and a single exponential fit. Far better agreement was observed using a double exponential fit. The double exponential curve fits were applied between data points where the signal intensity was 10% and 90% of the peak value. The cooling process of the laser-heated soot reflects the concurrent contributions of radiation, conduction, and convention that vary with time after the excitation laser pulse (*7-12*). Thus, the dual time constants may reflect different timescales associated with the different cooling mechanisms. Using the fast decay rate did not give a monotonic relation with increasing primary particle size. Figure 2 plots the second decay rate value (obtained by fitting the time-resolved LII signals for the various diffusion flames) against their primary particle size. The dynamic range and monotonic relationship exhibited by the analysis methods whose results are plotted in Figure 2 give each potential as an empirical calibration curve for inferring primary particle size based on the temporal decay rate of the LII signal in other systems.

### Application

Motivated by the need for measuring primary particle size to determine soot mass growth and oxidation rates per unit surface area (*1-6*), we tested the utility of the calibration curve for determining primary particle size. Time-resolved LII data were obtained at different heights above the burner along the axial streamline within the

ethylene flame and subsequently fit to a double exponential and also analyzed using the method of gate ratios. Using the calibration curves presented in Figure 2, the measured long-time decay rates were translated into primary particle sizes.

The trend exhibited in both calibration plots is similar to the predicted results published in reference 10. Although the acetylene point is consistent with this trend, it was not used because of the different flame temperature which will affect the cooling processes (see Table 1). Given the uncertainty in the functional form of a curve-fit, line segments connecting the calibration points were used for interpolation. The ethane-ethylene segment was extrapolated to obtain primary particle sizes from points beyond the ethylene calibration point.

Figure 3 presents the results. In order to test the accuracy of the predictions, thermophoretic sampling measurements were performed followed by TEM microscopy and subsequent primary particle size analysis. These results are also plotted in Figure 3. While good agreement is observed at heights above the burner (HAB) of 40, 45, 80, and 85 mm, pronounced differences exist between 55 and 75 mm HAB, where the values measured from the TEM micrographs are significantly below the predicted values. Note that the agreement observed at 50 mm reflects its being used as a calibration point.

The deviations observed in the oxidation regions likely result from the aerosol process of cluster-cluster aggregation (14). Soon after the formation of aggregates within the growth region, clustering of aggregates can begin. This process will continue to occur throughout the growth and well into the oxidation regions of the flame. TEM images in the annular region of the flame show that as the aggregates cluster, they not only become larger but also more dense and compact (15,16). This is consistent with our own observations along the axial streamline. TEM images of soot aggregates collected at 40, 60, and 80 mm HAB show that the open branched chain appearance of aggregates within the growth region do qualitatively change to a more densely-packed, less open structure in the oxidation region. Such a structure could decrease the rate of cooling of individual primary particles (or fused units) through self-absorption of emitted thermal radiation and inhibition of conductive and convective cooling. Hence the optical measurement, which reflects the rate of temperature decrease of the laser-heated soot, would also be affected. Upon sufficient oxidation, the aggregates eventually crumble, so that the primary particles within the fragments return to a more open structure similar to that at their initial coalescence early within the growth region. At this stage, good agreement between the optical and TEM measurements would be expected, as observed. It could be argued that the oxidation process itself could slow the rate of cooling of the laser-heated soot. Localized burning of the soot could contribute to locally elevated temperatures of the particles. Given the agreement between temperatures within sooting flames measured via optical pyrommetry and thermocouples, however, this appears to be a minor contribution.

Another soot particle property that could affect the cooling process is the degree of primary particle connectivity. The degree of connectivity is a maximum at the peak of the soot growth region. Increasing primary particle connectivity would increase the effective primary particle size thus decreasing the cooling rate. Since our calibration points are at the peak of the growth region where the connectivity effects are maximum, this would underpredict primary particle sizes at other heights. The observed agreement between the predicted and experimental results within the soot growth region and the fact that the predicted results lie above the TEM measured values indicate that primary particle connectivity does not significantly impact the results presented here. The overprediction of the primary particle size relative to the TEM values within the oxidation region is also consistent with this postulate.

## CONCLUSIONS

Our results suggest that LII can be used to predict primary particle size under certain conditions. Local flame temperatures will affect the cooling rate of the particle and thus the optical signal. Therefore, the flame temperature in the calibration system and the system to which it is applied must be similar in this empirical approach. Cluster-cluster aggregation will also affect the cooling rate

and the predicted primary particle sizes if it differs between the two systems. Particle-particle connectivity does not appear to be a significant factor in the results presented here.

These results represent the first direct comparison between primary particle sizes based on optical measurements and those directly measured through TEM. Predictions based on the temporal decay rate of the LII signal produce better agreement than those based on the gate ratio method.

## ACKNOWLEDGEMENTS

## REFERENCES

1. Harris, S.J.; Weiner, A.M. *Combust. Sci. and Technol.* **1984**, *38*, 75.
2. Megardis, C.M. *Combust. Sci. and Technol.* **1989**, *66*, 1.
3. Sunderland, P.B.; Faeth, G.M. *Combust. and Flame* **1996**, *105*, 132.
4. Sunderland, P.B.; Koylu, U.O.; Faeth, G.M. *Combust. and Flame* **1995**, *100*, 310.
5. Frenklach, M.; Wang, H.   23rd Symposium (International) on Combustion, The Combustion Institute, Pittsburgh, PA. 1990; 1559.
6. Howard, J.B.; 23rd Symposium (International) on Combustion, The Combustion Institute, Pittsburgh, PA. 1990; 1107.
7. Melton, L.A. *Appl. Opt.* **1984**, *23*, 2201.
8. Hofeldt, D.L.   Society of Automotive Engineers, Warrendale, PA, 1993; SAE Tech. Paper 930079.
9. Dasch, C.J. *Appl. Opt.* **1984**, *23*, 2209.
10. Mewes, B.; and Seitzman, J.M. *Appl. Opt*, **1997**, *36*, 709.
11. Will, S.; Schraml, S.; and Leipertz, A. 23rd Symposium (International) on Combustion, The Combustion Institute, Pittsburgh, PA. 1996; 2277.
12. Eisner, D.A.; Rosner, D.E. *Combust. and Flame*, **1985**, *61*, 153.
13. Smyth, K.C.; Miller, J.H.; Dorfman, R.C.; Mallard, W.G.; Santoro, R.J. *Combust. and Flame*, **1985**, *62*, 157.
14. Puri, R.; Richardson, T.F.; Santoro, R.J.; *Combust. and Flame*, **1993**, *92*, 320.
15. Dobbins, R.A.; Megaridis, C.M. *Langmuir* **1987**, *3*, 254.
16. Koylu, U.O.; Faeth, G.M.; Farias, T.L.; Caravalho, M.G. *Combust. and Flame*, **1995**, *100*, 621.

| Fuel | Flow Rate (sccm) | Axial Height (mm) | Primary Size TEM (nm) | Temperature (K) |
|------|------------------|-------------------|-----------------------|-----------------|
| Methane | 350 | 50 | 13.4 +/- 1.6 | 1750 |
| Ethane | 255 | 61 | 24.4 +/- 2.1 | 1700 |
| Ethylene | 231 | 50 | 33.3 +/- 3.5 | 1600 |
| Acetylene | 200 | 50 | 59.7 +/- 3.9 | 1200 |

Table 1.   Summary of experimental conditions and primary particle sizes.
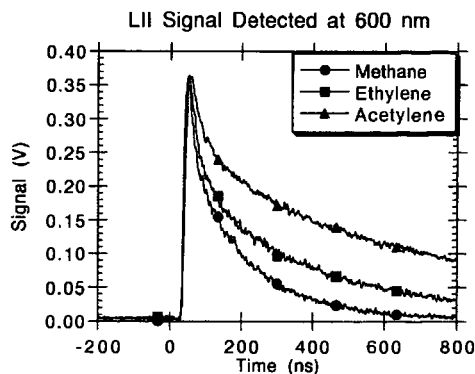
## LII Signal Detected at 600 nm

Figure 1. Time-resolved LII signals produced by the different size primary particles in the various flames.
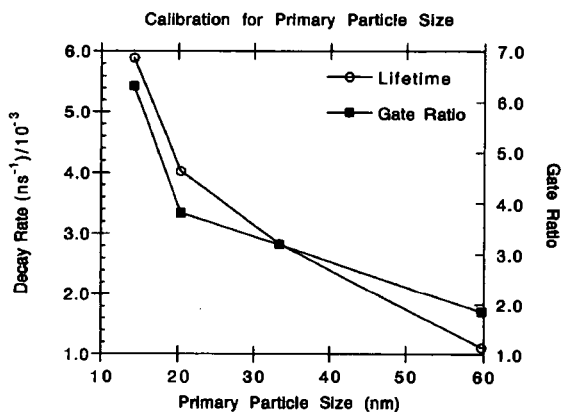
## Calibration for Primary Particle Size

Figure 2. Correlation between measured primary particle size and the second decay rate and gate ratio describing the temporally resolved LII signal.

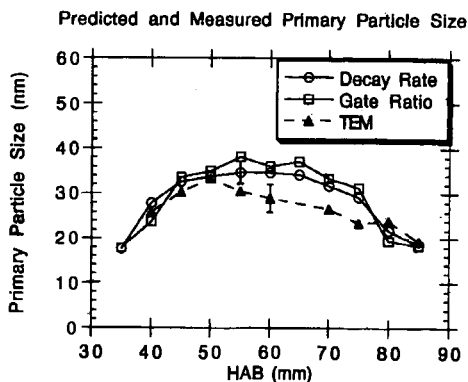## Predicted and Measured Primary Particle Size

Figure 3. Comparison between the predicted primary particle size based on the optical measurements and interpreted using the calibration curves in Figure 2 and direct measurements from TEM micrographs.

# OPTIMIZATION OF THERMAL CRACKING UNIT WITH AUTOMATIC HEAVY FUEL OIL STABILITY ANALYZER

Olli Pilviö[1] , Juha Vilhunen [2] ,Jouni Tummavuori[3]
[1] Neste Oy, Corporate Technology, PO Box 310, FIN 06101 Porvoo, Finland
[2] Finnish Measurement Systems FMS Ltd, Tekniikantie 21 A, FIN-02150 Espoo, Finland
[3] University of Jyväskylä, Dept. of Chemistry, PO Box 35, FIN 40351 Jyväskylä, Finland

**Keywords:** heavy fuel oils, stability, analyzer

## ABSTRACT

The main target in optimizing the thermal cracking unit is to maximize the yield of the valuable lighter intermediate distillates. The cracking process is then running as near as possible but still on the safe side of the severity limit resulting stable fuel oil. Stability or long storage life is an important factor demanded of heavy fuel oils refined in the thermal cracking/visbreaking production units. The stability figure for heavy fuel oils indicates the precipitation tendency of asphaltene molecules in the oil. The stability parameters (P-value, toluene or xylene equivalents) are usually determined by the manual spot test method using visual detection. However, these tedious manual methods take up to hours to perform.

PORLA, an automatic stability analyzer for heavy fuel oils[1,2] was developed and has been used for several years by a Finnish oil company Neste Oy. The stability analyzer performs the same stability measurement procedure (determination of P-value) as the manual method only in few minutes. The laboratory model of the instrument is now commercially available and it has also been tested in the laboratories of other oil companies. There is a good correlation between the results obtained by the analyzer and those by the manual method. The automatic stability analyzer brings with a cost-effective and reliable tool for optimization of thermal cracking processes and blending of heavy fuel oil components.

## INTRODUCTION

An important prerequisite for the hassle-free use of heavy fuel oils is that there exist no precipitate formation during their storage and use. The formation of the precipitates in oils is a consequence of flocculation of the asphaltenes present in the oil. The amount and quality of asphaltene particles in the oil and the production conditions determine the tendency for asphaltene precipitation. The stability figure is depending on quality of the feed stock, the reactor temperature and reactor residence time. Stability figures (P-value, peptization value, xylene or toluene equivalent) all describe the precipitation tendency of the asphaltenes. One of the stability figures p value is an abstract real number varying between 1 and 6.

In oil refining, the thermal cracking processes are adjusted such a way that the bottom products are always stable. The optimal temperature of thermal cracker unit is decisive. The profitability of thermal cracking unit improves as the quantity of valuable middle-distillates such as light fuel oil and diesel fuel components increase. The yield of these components is maximized by control of process temperature. If the process temperature is too low, part of the middle-distillates remain in the heavy fuel oils and production is not optimal. If again the process temperature is too high, that results in unstable products, which will sedimentate during storage or upon mixing with other oils.

In general, when the stability figure is about two the production economics is optimized; the yield of the valuable light and middle-distillate components are maximized and the heavy fuel oil is still stable without any remarkable addition of expensive "solvents" (light gas oil components). P values near 1 mean unstable products.

However, the optimal P-value for each process varies, because the products can be used for different applications. For some applications, however, a sufficient P- value for the product is even 1.5 and in some applications it must be near 2, it depends on the blending. In case of e.g. marine applications, where wide range of blending may take place, the sedimentation of aphaltenes may result in engine problems due to clogging of ship's fuel system (separators and filters). To prevent asphaltene precipitation in oil products refined at too high temperature, "solvents" have to be added. Solvents are however expensive and production economy suffers. Therefore, the range between 1.5 and 2 is the area where the optimization of the process and the product with help of the P-value determination can bring huge amounts of money to oil refining companies. 0.5 P-value units may mean millions of US dollars annually, depending on the capacity and feed stock of the refinery. The P-values above two mean "too good" products which will seldom cause any stability problems, but that is at the expense of the production economy.

In practice, the optimal process temperature of thermal cracker unit is set at safe distance from, but as close to the upper temperature limit as possible. The automatic stability analyzer method, which gives the stability figure in few minutes, will be presented. The instrument was developed to replace the tedious manual methods in order to regulate the optimal process temperature especially when changing the feed stock in the production.

## EXPERIMENTAL

### Determination of stability figures

The stability parameter is usually determined by manual spot test method using visual detection. In order to adjust the viscosity of the heavy fuel oil sample be aromatic solvent likc xylene or toluene is added. The asphaltenes in the heavy oil sample are precipitated by gradual addition of paraffinic solvent like n-heptane, decane or iso-octane. When subsequent amount of paraffinic solvent is added the oil becomes unstable and asphaltenes precipitate. After each addition of paraffinic solvent a droplet of the solution is placed on a filter paper and the visual detection of the two dark rings within each other formed in the spot indicate the precipitation. The stability parameter is determined from the amounts of oil, paraffinic and aromatic solvents. This manual test procedure takes from one to two hours to perform.

The function of an automatic computer controlled analyzer is based on the same procedure as the manual method, and the optical detection of precipitation point of asphaltenes during the measurement procedure is based on the scattering of visible light. At the precipitation point the intensity of scattered light rapidly increases. The analyzer gradually adds the selected paraffinic solvent in the prediluted heavy fuel oil sample, detects optically the precipitation point of asphaltenes and finally calculates the stability figure (P-value) on the basis of mass of the oil and the volume of aromatic solvent and paraffinic solvent consumption. To calibrate the instrument, three different dilutions from a heavy fuel oil with known P-value are first run by the instrument. Typical oil/aromatic solvent ratios are 4/1, 4/2, 4/3. The stability figures of these three solutions are applied in extrapolation procedure, where the impact of aromatic solvent to the solubility of asphaltenes is eliminated.

When all three solutions have been run by the analyzer the consumption of paraffinic solvent e.g. heptane of the undiluted heavy fuel oil sample $X_0$ can be extrapolated with the following way[3]:

$Y$ = xylene (ml) / [xylene (ml) + n-heptane (ml)]

$X$ = oil (g) / [xylene (ml) + n-heptane (ml)]

Figure 1 schematically illustrates the extrapolation procedure based on the titration of the three dilutions resulting paraffinic solvent consumption of an undiluted oil sample. Consequently, the stability figure P-value is calculated from the following equation:

$$P = 1 + 1/X_0,$$

where $X_0$ is the intersection of x axis and the straight line extrapolated via the three data points.

### Correlation of P-value and toluene/xylene equivalents

In addition to the P-value, other methods like toluene and xylene equivalents are used to determine the stability of heavy fuel oils. Toluene and xylene equivalents are equal, the only difference between these two methods is the solvent (toluene/xylene). Toluene equivalent is determined by a method where the heavy fuel oil sample is first mixed with toluene typically in the proportion of one to five. Paraffinic solvent is gradually added in the mixture. After every paraffinic solvent addition a droplet of the mixture is taken and placed on a filter paper until separation of the spots appear. The toluene equivalent is the lowest toluene concentration (expressed in vol-%) of the solution where the asphaltenes are not precipitated[3]. The toluene/xylene equivalent is calculated in the following way:

Tol-eq. ={toluene (ml) / [toluene (ml) + n-heptane (ml)]}*100 %

When comparing the equation for the calculation of toluene equivalent and that one for the Y axis of the P-value determination the correlation between P-value and toluene equivalent can be seen. Figure 2 illustrates this linear correlation.

### RESULTS

In an eight months laboratory monitoring test carried out by Scanraff refinery in Sweden[4] almost one hundred heavy visbreaker fuel (Vistar) oil samples with same origin were analyzed both manually and automatically with the analyzer. One objective of this test was to check correlation between the analyzer and the manual spot test method in the oil quality control laboratory use. The original values of this test period can be seen in Table 1. Fig 3 shows the stability figures for product "Vistar" obtained by PORLA and the deviations from the manual method during the monitoring period. 73 samples of 93 gave exactly the same stability figure by both methods, 8 samples gave 0.1 P-value unit higher value and 12 samples 0.1 P-value unit lower value by the analyzer than by the manual method. The statistical testing of the analyzer during over decade's constant use in refinery laboratories has proven the repeatability of the analyzer to be ±0.05 P-value unit. The test run result confirmed our repeatability results.

The results obtained by manual and automated methods did not significantly differ from each others. This is shown on the basis of the statistical tests carried out from the original data of Table1. The statistical tests done were F-test (Two-Sample for Variances), t-test (Paired Two-Sample for Means) and Friedman test (Repeated Measures Analysis of Variance on Ranks).

Probability value 0.40 of F-test shows variances to be equal. Paired t-test of which critical t-value was $1.98_{0.05}$ gave t-value 0.61 and probability 0.53. To confirm the test results obtained by F-test and t-test the Friedman test (Repeated Measures Analysis of Variance on Ranks) was performed. Table 2 shows and figure 4 illustrates the result of Friedman test. The differences in the median values among the treatment groups are not great enough to exclude the possibility that the difference is due to random sampling variability; there is not a statistically significant difference between manually and automatically obtained results of P-values.

Especially the process temperature affects the formation and precipitation tendency of asphaltene particles. It is essential to control the reactor temperature of a thermal cracker production unit to such a level, where the heavy oil produced is still stable and there is no coke formation in the reactor tubes. A typical correlation between the temperature of thermal cracker reactor and the stability figure (P-value) for certain crude oil feed stock is illustrated in figure 5. The optimum reactor temperature, however, may vary according to the feed stock material and therefore it is important to detect for every feed stock the stability limit, which corresponds the highest temperature, where the production is on the safe side, where the product is stable and as near as possible to the severity limit in order to optimize the yield of the valuable lighter products and to avoid coke formation, which may lead to interruption of the production.

## CONCLUSIONS

The optimization of thermal cracker units and the quality control of heavy fuel oil production can be improved as minimized off-spec production by an automated stability analyzer. Additionally, the use of an automatic analyzer brings with remarkable labor cost savings in an oil quality control laboratory compared to the tedious manual methods. Besides, the automated analyzer minimizes the errors due to differences in individual human capabilities for visual detection of spot test.

An automated stability analyzer developed at Neste oil refinery in Finland is based on this manual test method, but it performs the same procedure automatically in few minutes. It has been developed in order to save oil refinery laboratories' labor costs and to improve the handling of heavy oil stability and quality control.

It is known that the wider the dissimilarity between the blend components, the greater is the risk of incompatibility and possible often significant economical consequences. This automated method can be used also for detecting the stability figure of heavy fuel oil blends i.e. binary or ternary systems. Some stable products may form an unstable blend. Therefore, it could be reasonable to check beforehand the stability of such blends by making stable/unstable maps for binary or ternary heavy fuel oils systems.

Statistical calculations of the Scanraff's test run results indicate that there are not statistically significant differences between the result obtained by the manual and automated method. The small differences in the results is if anything due to random sampling variability. Therefore, the automatic method offers an fast, cost-effective and reliable tool to replace the tedious manual methods for analyzing the stability figure of heavy fuel oils.

## REFERENCES

1. O.Pilviö, "Automatic Stability Analyzer of Heavy Fuel Oils", IASH '94, the 5th International Conference on Stability and Handling of Liquid Fuels, October 3-7, 1994, Rotterdam, the Netherlands
2. O.Pilviö, J.K.Vilhunen and L.-Å. Larsson., "Experiences in Use of Automatic Heavy Fuel Oil Stability Analyzer", IASH '97, the 6th International Conference on Stability and Handling of Liquid Fuels, October 12-17, 1997, Vancouver, B.C., Canada
3. R.Kassinger, "Fuel Blending - How to Minimize Risk of Incompatibility", IASH '97, the International Conference on Stability and Handling of Liquid Fuels, October 12-17, 1997, Vancouver, B.C., Canada
4. L.-Å.Larsson, Test run report of Porla analyzer January 1997, Scanraff, Lysekil, Sweden

TABLE 1. Stability figures P-values obtained manually and by automated PORLA analyzer during eight months test period at Scanraff, Sweden.

| Manual | Automat | Manual | Automat | Manual | Automat | Manual | Automat |
|--------|---------|--------|---------|--------|---------|--------|---------|
| 1.7 | 1.7 | 2.0 | 2.0 | 2.0 | 2.0 | 2.0 | 2.0 |
| 1.9 | 1.9 | 2.1 | 2.0 | 2.0 | 2.0 | 2.1 | . 2.1 |
| 1.9 | 2.0 | 2.4 | 2.3 | 2.0 | 2.0 | 2.0 | 2.0 |
| 1.8 | 1.8 | 1.9 | 1.9 | 2.0 | 2.0 | 2.0 | 2.0 |
| 1.8 | 1.8 | 2.5 | 2.5 | 2.0 | 2.1 | 2.1 | 2.1 |
| 1.9 | 1.9 | 2.1 | 2.1 | 2.0 | 2.0 | 2.1 | 2.1 |
| 1.9 | 2.0 | 2.6 | 2.6 | 1.8 | 1.8 | 2.1 | 2.0 |
| 2.0 | 1.9 | 2.0 | 2.0 | 2.0 | 2.0 | 2.2 | 2.2 |
| 2.1 | 2.0 | 2.0 | 2.0 | 1.8 | 1.8 | 2.3 | 2.4 |
| 1.7 | 1.6 | 2.0 | 2.0 | 2.0 | 2.0 | 2.0 | 2.0 |
| 1.6 | 1.6 | 2.0 | 2.0 | 2.1 | 2.1 | 1.9 | 1.9 |
| 1.6 | 1.6 | 2.1 | 2.1 | 2.0 | 2.0 | 2.1 | 2.1 |
| 2.3 | 2.2 | 1.8 | 1.7 | 1.9 | 1.9 | 2.1 | 2.1 |
| 1.6 | 1.6 | 1.8 | 1.7 | 1.9 | 1.9 | 2.0 | 2.1 |
| 1.6 | 1.6 | 1.9 | 1.9 | 1.7 | 1.8 | 2.1 | 2.1 |
| 2.2 | 2.1 | 1.8 | 1.8 | 1.9 | 1.9 | 2.1 | 2.1 |
| 2.2 | 2.2 | 1.8 | 1.8 | 1.9 | 1.9 | 2.1 | 2.1 |
| 1.9 | 1.9 | 2.0 | 2.1 | 1.7 | 1.7 | 2.0 | 2.0 |
| 2.1 | 2.1 | 2.2 | 2.1 | 2.0 | 2.0 | 2.1 | 2.1 |
| 2.1 | 2.1 | 1.9 | 1.9 | 2.0 | 2.1 | 2.0 | 2.0 |
| 1.9 | 1.8 | 1.8 | 1.8 | 2.3 | 2.3 | 2.1 | 2.1 |
| 2.2 | 2.2 | 1.8 | 1.8 | 2.0 | 2.0 | | |
| 2.1 | 2.1 | 2.1 | 2.1 | 2.0 | 2.0 | | |
| 2.2 | 2.2 | 2.0 | 1.9 | 2.0 | 2.0 | | |

TABLE 2. The results of Friedman test from the values of table 1.

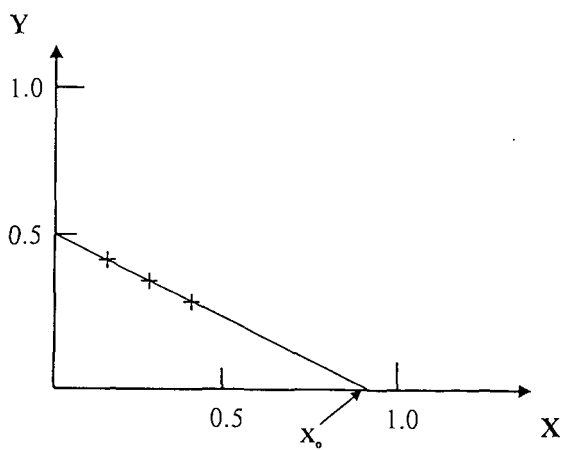| Group | Median | 25 % | 75 % |
|-------|--------|------|------|
| Manually | 2.0 | 1.9 | 2.1 |
| Automatic | 2.0 | 1.9 | 2.1 |
| Chi-square = 0.667 with 1 degrees of freedom. (P = 0.4142) | | | |

FIGURE 1. Determination of paraffinic solvent consumption for an undiluted heavy fuel oil sample $X_0$ by extrapolation.
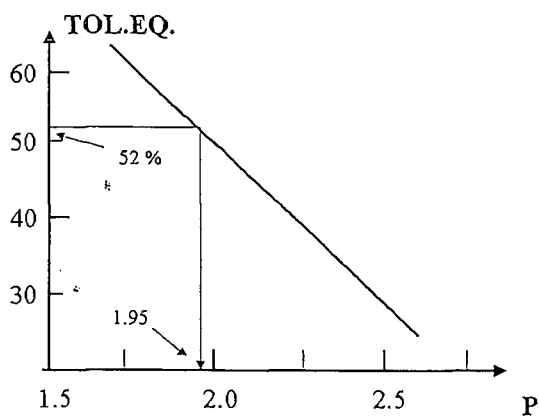
Figure 2. Linear correlation between toluene equivalent and P-value for heavy fuel oils.
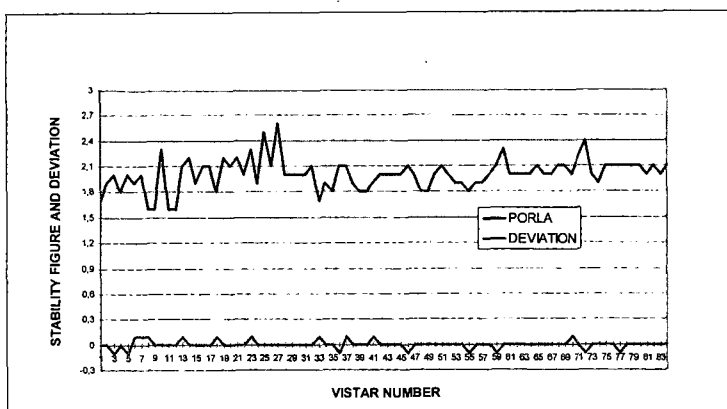
FIGURE 3. Stability figures of Vistar heavy fuel oil product obtained by PORLA analyzer and deviation of each value from the manually obtained value.
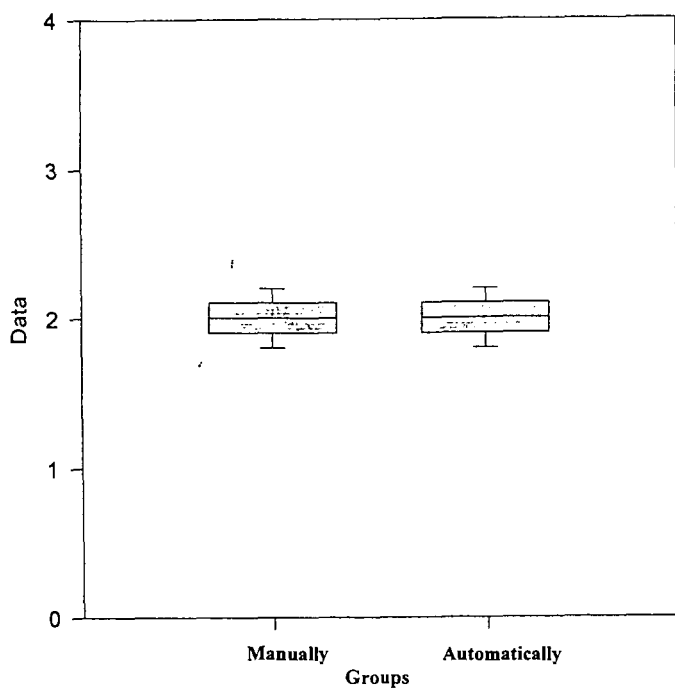
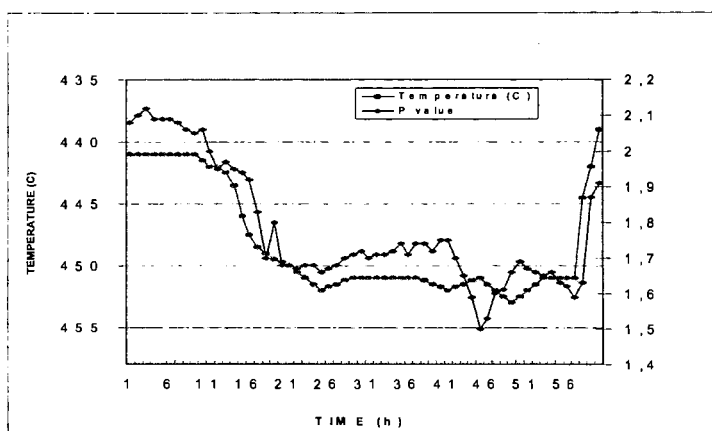FIGURE 4. A graphical illustration of the result of Friedman test carried out from the data of table 1.

FIGURE 5. Correlation between stability figure and thermal cracking process for certain feed stock material.